crystals

MDPI

Article

Excited State Calculations of Cu-Doped Anatase TiO_2 (101) and (001) Nanofilms

Yin-Pai Lin [1], Elina Neilande [1,*], Hanna Bandarenka [2], Siarhei Zavatski [2], Inta Isakoviča [1], Sergei Piskunov [1], Dmitry Bocharov [1,*] and Eugene A. Kotomin [1,*]

[1] Institute of Solid State Physics, University of Latvia, 8 Kengaraga Street, LV-1063 Riga, Latvia; intai@cfi.lu.lv (I.I.); piskunov@cfi.lu.lv (S.P.)
[2] Applied Plasmonics Laboratory, Belarusian State University of Informatics and Radioelectronics, 6 Brovka Street, 220013 Minsk, Belarus; h.bandarenka@bsuir.by (H.B.); s.zavatskij@bsuir.by (S.Z.)
* Correspondence: elina.neilande@cfi.lu.lv (E.N.); bocharov@cfi.lu.lv (D.B.); kotomin@cfi.lu.lv (E.A.K.)

Abstract: Excited state calculations are performed to predict the electronic structure and optical absorption characteristics of Cu-doped anatase TiO_2 nanofilms, focusing on their (101) and (001) surface terminations. Using model structures that successfully represent the equilibrium positions of deposited Cu atoms on the TiO_2 surface, a comprehensive analysis of the absorption spectra for each considered model is made. The proposed modeling reveals phenomena when photogenerated electrons from TiO_2 tend to accumulate in the vicinity of the deposited Cu atoms exposed to photon energies surpassing the band gap of TiO_2 (approximately 3.2 eV). The crucial transition states that are essential for the creation of potential photocatalytic materials are identified through detailed calculations of the excited states. These insights hold substantial promise for the strategic design of advanced photocatalytic materials. The obtained results provide a base for subsequent analyses, facilitating the determination of heightened surface reactivity, photostimulated water splitting, and antibacterial properties.

Keywords: TiO_2 nanofilm; photocatalyst; Cu dopant; time-dependent density functional theory; absorption spectra

Citation: Lin, Y.-P.; Neilande, E.; Bandarenka, H.; Zavatski, S.; Isakoviča, I.; Piskunov, S.; Bocharov, D.; Kotomin, E.A. Excited State Calculations of Cu-Doped Anatase TiO_2 (101) and (001) Nanofilms. *Crystals* **2024**, *14*, 247. https://doi.org/10.3390/cryst14030247

Academic Editor: Antonio Frontera

Received: 3 January 2024
Revised: 21 February 2024
Accepted: 25 February 2024
Published: 1 March 2024

1. Introduction

In recent decades, heterogeneous photocatalysis has emerged as a promising pathway for advancing green technologies, particularly in the domains of photocatalytic water splitting, the degradation of hazardous organic pollutants, and the manifestation of robust antibacterial properties [1,2]. The comprehensive investigation underscores the significance of TiO_2-based materials, attributing their appeal to environmentally benign attributes such as non-toxicity, stability, cost-effectiveness, and wide-ranging applicability [3–15]. Central to photocatalysis are mechanisms involving the generation of photogenerated charges, encompassing processes such as photo-induced charge separation, bulk and surface charge recombination, and surface charge reactions [16]. Subsequently, photogenerated electron–hole pairs engage with water, hydroxide groups, and molecular oxygen adsorbed on the TiO_2 surface, yielding reactive oxygen species such as superoxide anions and hydroxyl radicals. These reactive oxygen species play a pivotal role in oxidation reactions that detrimentally affect the cell membranes, ribonucleic acid (RNA), deoxyribonucleic acid (DNA), proteins, lipids, and other cellular components, ultimately causing the demise of microorganisms [17,18].

Despite the numerous merits of TiO_2, its wide band gap (ranging from 3.0 to 3.2 eV [19]) limits efficient photoabsorption in the visible light region of the solar spectrum. To overcome this, integrating 3*d* metal dopants, such as copper [3,4,16,20], into TiO_2 has shown promise in boosting both its photocatalytic and antibacterial capabilities [21–23]. Copper

introduces improvements by mitigating electron–hole pair recombination, thereby extending the lifespan of electrons and concurrently improving the photoresponse under visible light irradiation [18].

Although titanium dioxide has been the subject of wide experimental [9,24–30] and theoretical [31–35] investigations, the full scope of its photocatalytic and antibacterial properties, as well as their potential enhancements, remains an open field for exploration. State-of-the-art spectroscopy can analyze electronic structure at the atomic scale, including binding energies [36,37] and imaging reaction sites [38]. Nevertheless, the technology for synthesizing photocatalysts is still in need of improvement. From an experimental standpoint, measuring the absorption spectra of photocatalysts offers insights into solar energy utilization efficiency [36,37,39,40].

Experimentally probing photon-induced electron transitions in single atoms or small clusters on semiconductor surfaces holds great promise, yet it is notably challenging, largely due to various constraints [4]. However, the swift advancement in computer technologies and the growing capabilities of supercomputers have globally opened new avenues for theoretical studies. These studies leverage quantum chemistry and density functional theory (DFT) as important tools for exploring charge transitions and photoabsorption at an atomic level. Time-dependent DFT (TDDFT) is an extension of density functional theory (DFT). The integration of TDDFT with the linear combination of atomic orbitals (LCAO) method has enabled simulations of structures comprising up to hundreds of atoms [41–43]. While DFT focuses on ground-state properties, TDDFT allows for the study of excited states and time-dependent phenomena. This approach achieves a balanced compromise between accuracy and computational efficiency. Moreover, the time propagation feature in LCAO TDDFT allows for the effective breakdown of Kohn–Sham wave functions. This breakdown is instrumental in representing transition states at specific energy levels. It could be used to simulate how electronic systems evolve over time under various conditions, such as in response to an external electromagnetic field providing a practical means to present the transition behavior from occupied to unoccupied Kohn–Sham orbitals [41–44].

Recent literature reviews [36,37,39] highlight the advantageous effects of noble metal clusters on the TiO_2 surface, significantly boosting absorption in the photon spectrum ranging from visible to ultraviolet light. This enhancement of the absorption is primarily attributed to electron transitions within these noble metal clusters, which lead to the formation of excited states in the system. In the realm of TDDFT, the ground states are usually consistent with either structures that are optimized or those that represent minimal interactions among the components on the surface, as indicated in references [39,45]. However, there are geometric configurations that are close to the minimum energy of equilibrium models and that still fulfill the criteria for convergence in DFT calculations. Although the absorption spectrum might display similarities across different geometries, variations in the electronic orbitals due to such different geometries could cause noticeable differences in the localization patterns of the transitions [23].

In this paper, we perform the first-principles analysis of the optical absorption characteristics of Cu-doped anatase TiO_2 surfaces, with a focus on the (101) and (001) surface terminations. The (101) and (001) surfaces of anatase TiO_2 are the most thermodynamically stable and reactive surfaces, respectively. The (101) surface, being the most stable, is commonly observed in naturally occurring and synthetic anatase TiO_2 particles. Its stability is crucial for applications that require long-term durability. The (001) surface, on the other hand, exhibits higher reactivity, making it particularly interesting for catalytic applications. The distinct properties of these surfaces influence the interaction with dopants like Cu, potentially altering the electronic structure and enhancing the material's photocatalytic efficiency [10]. The study aims to predict and analyze the electronic structure of Cu-doped TiO_2 surfaces and involves examining how the presence of copper dopants affects the electronic states and energy levels at the TiO_2 surface; to examine the optical absorption properties of these structures to understand how the introduction of copper atoms affects the material's ability to absorb light, particularly in the visible spectrum, which is crucial

for photocatalytic applications; as well as to identify and discuss the crucial transition states and their implications for advanced photocatalytic material development. These states are important for understanding the behavior of photogenerated electrons in the presence of copper atoms and for the development of future photocatalytic materials.

2. Computation Details

The calculations in this study were performed using GPAW software [46,47], along with the Atomic Simulation Environment (ASE) library [48]. The electronic configurations of valence electrons for oxygen, titanium, and copper were specified as O($2s^2 2p^4$), Ti($3s^2 3p^6 3d^2 4s^2$), and Cu($3d^{10} 4s^1$), respectively. Specifically, oxygen atoms were analyzed using the default Projector Augmented-Wave (PAW) dataset, version 0.9.20000, and the double-ζ polarized (dzp) basis sets provided in the GPAW package. To ensure precise modeling of absorption processes, both titanium and copper atoms were treated using the optimized double-ζ basis sets (p-valence) [49,50]. A critical aspect of these basis sets is their construction: for p-valence, the Gaussian polarization function, typically seen in dzp, is replaced with a bound, unoccupied p-type orbital and a split-valence wave function, providing a more accurate representation of the atomic orbitals.

The study is focused on a detailed examination of the pristine anatase TiO_2 surfaces, specifically the (101) and (001) facets. The (101) surface, consisting of 72 atoms (24 titanium and 48 oxygen atoms, slab thickness 9.2 Å), and the (001) surface, with 108 atoms (36 titanium and 72 oxygen atoms, slab thickness 9.1 Å), were modeled by slicing the bulk anatase crystal along the (101) and (001) directions. For the (101) surface, two distinct models were conceptualized (as shown in Figure 1b,c), due to variations in the positions of atoms used to cut the boundary in the x direction. To simulate an infinite surface, the periodic boundary conditions were applied in the x and y directions, while a substantial vacuum gap of 15 Å was introduced along the z direction to avoid interactions between the surfaces of the slab.

The vacuum gap of 15 Å has been kept fixed during the atomistic optimization procedure.

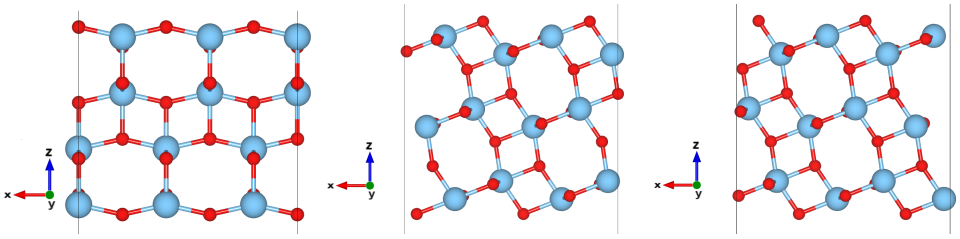

(**a**) (**b**) (**c**)

Figure 1. Schematic atomic structure of the anatase TiO_2 surface: (**a**) (001) slab, (**b**) (101) type A, and (**c**) (101) type B. Oxygen and titanium atoms are represented by colored balls in red and blue, respectively.

Structural optimization was performed using the Broyden–Fletcher–Goldfarb–Shanno (BFGS) algorithm, which is widely used in numerical optimization, particularly for solving unconstrained nonlinear optimization problems [51]. It belongs to a class of iterative methods known as quasi-Newton methods, which are designed to find local minima or maxima of functions. At each step, it uses the gradient (first-order derivatives) of the function and an approximate inverse Hessian matrix to determine the next point to evaluate, without the need to compute the Hessian matrix (second-order partial derivatives of the function) directly. The key feature of BFGS is its way of updating the inverse Hessian matrix. It uses information from the gradient to refine this approximation at each step, making it more efficient than calculating the true Hessian.

For optimizing atomic coordinates, a grid-spacing parameter of 0.2 Å and the Perdew–Burke–Ernzerh (PBE) [52] exchange-correlation functional were employed to evaluate electronic densities and potentials. The *k*-point meshes, critical for sampling the Brillouin zone, were set at $3 \times 3 \times 1$ following the Pack–Monkhorst scheme. The optimization process was deemed complete when the maximal force on any atom was reduced to below 0.05 eV/Å.

For the electronic structure's ground state calculations, the linear combination of atomic orbitals (LCAO) method was utilized [53], incorporating the Gritsenko–van Leeuwen–van Lenthe–Baerends orbital-dependent functional, meaning it explicitly uses information from the Kohn–Sham orbitals, with a solid-state modification (GLLB-SC) [54]. One of the key advantages of the GLLB-SC functional is its ability to correct the self-interaction error, a common challenge in many traditional DFT functionals. Due to its strengths in band gap prediction and treatment of exchange-correlation energy, this functional is widely used in the study of the electronic properties of materials. The GLLB-SC functional also is computationally more efficient than many-body perturbation theories like GW approximation, making it a practical choice for larger systems [55]. To model dynamic electronic behavior, real-time propagated wave functions were generated for the surface models by applying a weak δ-kick of a dipole electric field in each Cartesian coordinate direction (x, y, and z). The propagation spanned 1500 time steps, each lasting 20 attoseconds, summing up to a total duration of 30 femtoseconds. The resulting time-dependent dipole moments were then transformed via Fourier analysis to create the absorption spectrum, utilizing Gaussian function broadening with a parameter $\eta = 0.07$ eV. The difference in absorption in the x–y and z directions stems from the reduced periodicity along the (z direction of the chosen multi-slab model). The visualization of pseudo-wave functions was conducted using VESTA software [56], and for comprehensive data analysis and the generation of graphical representations, Python's NumPy [57] and Matplotlib [58] packages were employed.

3. Results and Discussion

3.1. Pristine Surfaces

Computing the band gap of TiO_2 with the GLLB-SC functional provides a more accurate representation of titanium's *d*-orbitals. However, this method, which samples reciprocal space only at the Gamma point due to GPAW code constraints, can underestimate the band gap compared to experimental data and more comprehensive k-point sampling using the GLLB-SC functional. To address the noted discrepancy, the Hubbard DFT+U scheme is applied, enhancing the representation of localized electrons. The DFT+U methodology augments the standard DFT Hamiltonian with an additional term, known as the Hubbard U parameter [59]. This U term serves as a correction factor, specifically targeting the on-site Coulomb interactions among electrons in localized states, such as *d*- or *f*-orbitals. Its primary function is to impose an energy penalty on these systems when they exhibit fractional electron occupations. This penalty is designed to more accurately reflect the energetic cost associated with electron localization. In the context of this study, the adjustment of the Hubbard $U_{Ti(d)}$ parameter for titanium *d*-orbitals to 4.2 eV is implemented as recommended by Tritsaris et al. [60]. Table 1 illustrates the variance in the band gap for TiO_2 (101) and (001) surfaces, both with and without the application of the $U_{Ti(d)}$ parameter. Generally, instances where the Hubbard correction is applied exhibit larger band gaps compared to those without the $U_{Ti(d)}$ adjustment. On TiO_2 surfaces, the Hubbard correction induces a more pronounced localized attraction among electrons, effectively broadening the band gap.

Further, the electronic structure, specifically the density of states (DOS) for each case shown in Table 1, is graphically represented in Figure 2. The experimentally measured band gap for anatase TiO_2 is 3.2 eV. In comparison with these theoretical findings, the band gap of the TiO_2 (101) surface with the Hubbard correction tends to overestimate this value, while the TiO_2 (001) surface without the Hubbard correction underestimates it. This

discrepancy can be attributed to surface dangling bonds, as discussed by Deng et al. [61], which introduce additional states between the valence band maximum (VBM) and the conduction band minimum (CBM) that are absent in the bulk phase. Moreover, the TiO_2 (101) surface, having a reduced atomic count, presents fewer states, in contrast to the densely populated TiO_2 (001) surface.

Table 1. The band gap (in eV) calculated for (101)- and (001)-terminated pristine nanofilms of anatase TiO_2 with and without applied $U_{Ti(d)}$.

	$U_{Ti(d)} = 0$ eV	$U_{Ti(d)} = 4.2$ eV
TiO_2 (101) surface type A	3.32	4.18
TiO_2 (101) surface type B	3.31	4.17
TiO_2 (001) surface	2.55	3.39

The DOS calculated for the TiO_2 (101) surface shows distinct variations when comparing type A and B surfaces, both at $U_{Ti(d)}$ = 0 eV and 4.2 eV. For type A with $U_{Ti(d)}$ = 0 eV (Figure 2a), the DOS shows a baseline electronic structure that is significantly altered when $U_{Ti(d)}$ is increased to 4.2 eV (Figure 2b), indicating a shift in energy levels with the introduction of new states due to the potential applied. Similarly, for type B surfaces, the change in $U_{Ti(d)}$ from 0 (Figure 2c) to 4.2 eV (Figure 2d) reflects in the DOS due to the inherent differences between surface types A and B. These differences manifest in the energy distribution of states, the presence or absence of specific peaks, and the overall shape of the DOS curves. The DOS for the TiO_2 (001) surface at $U_{Ti(d)}$ = 0 eV (Figure 2e) and 4.2 eV (Figure 2f) provides a basis for comparison with the (101) surfaces. The (001) surface exhibits distinct electronic characteristics that are reflected in its DOS profile. The impact of applying $U_{Ti(d)}$ = 4.2 eV to the (001) surface offers insights into how different crystal orientations respond to electronic modifications. This comparison highlights the complexity and variability of the electronic structure in Cu-doped TiO_2 surfaces, emphasizing the importance of DOS analysis in understanding material properties for photocatalytic applications.

Applying the Hubbard correction to the band gap calculations for pure TiO_2 (101) surfaces, both types A and B (Figure 1b,c), affects their absorption spectra, leading to band gap increase. The absorption spectra of pure TiO_2 (101) surfaces with and without Hubbard correction are illustrated in Figure 3. When the Hubbard U parameter for titanium d-orbitals $U_{Ti(d)}$ = 4.2 eV is incorporated, the resulting optical absorption spectrum shows a red shift compared to neglect of the Hubbard correction. Interestingly, despite these adjustments, our analysis reveals that there is no significant difference in the absorption characteristics between the TiO_2 surfaces with and without the Hubbard correction [23,62,63]. This finding suggests that the Hubbard correction does not markedly alter the absorption properties of these surfaces, at least within the range of our study. To ensure a consistent approach in our study, we have opted to calculate the electronic structures of both pure and doped TiO_2 surfaces using the Hubbard correction $U_{Ti(d)}$ equal to 4.2 eV. This consistency in methodology allows for a more accurate comparison and understanding of the electronic properties across different TiO_2 surface configurations.

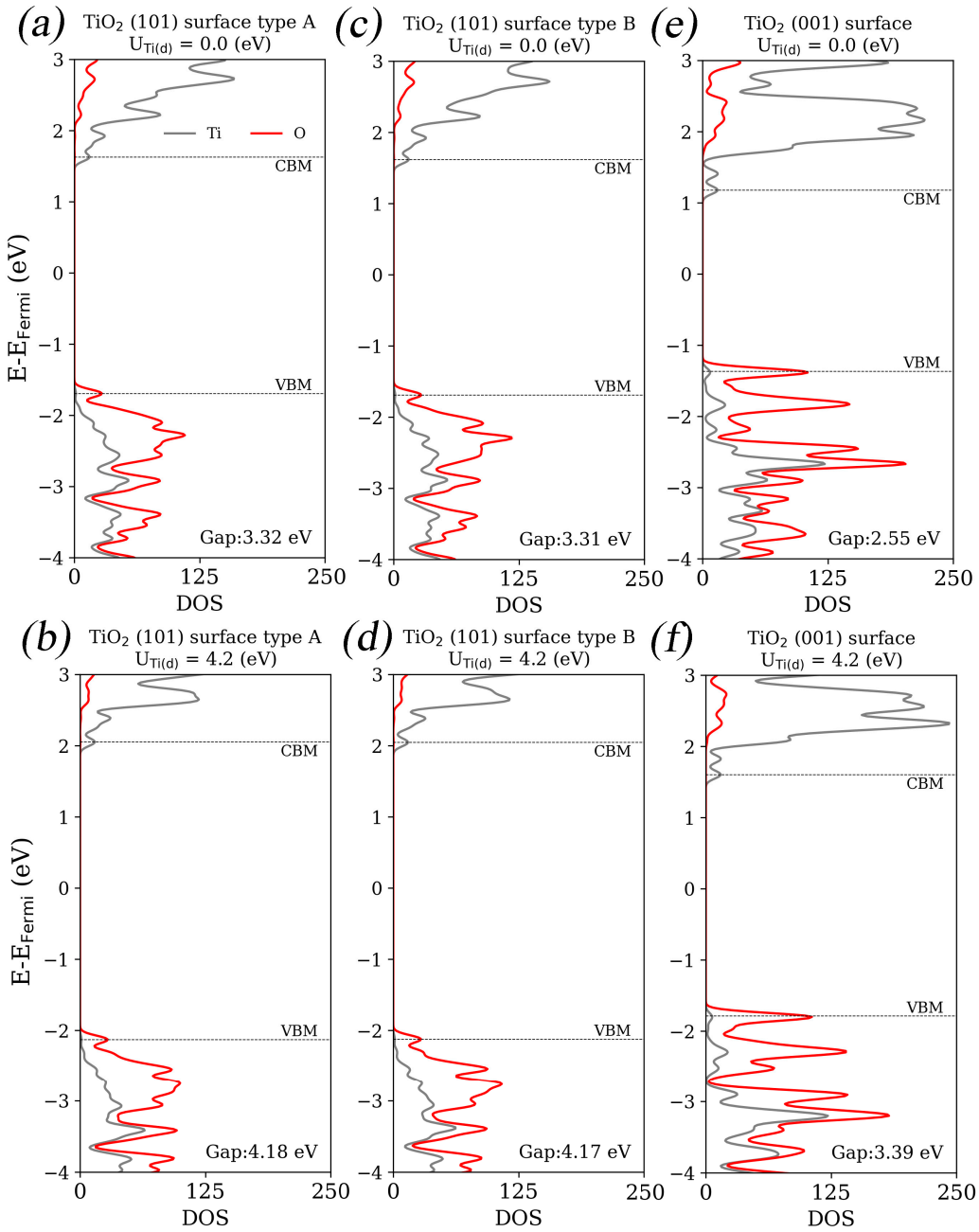

Figure 2. Density of states (DOS) calculated for (**a**) TiO_2 (101) surface type A with $U_{Ti(d)} = 0$ eV, (**b**) TiO_2 (101) surface type A with $U_{Ti(d)} = 4.2$ eV, (**c**) TiO_2 (101) surface type B with $U_{Ti(d)} = 0$ eV, (**d**) TiO_2 (101) surface type B with $U_{Ti(d)} = 4.2$ eV, (**e**) TiO_2 (001) surface with $U_{Ti(d)} = 0$ eV, and (**f**) TiO_2 (001) surface with $U_{Ti(d)} = 4.2$ eV (See Table 1). The lines in red and gray represent the DOS projected onto all orbitals of oxygen and titanium atoms, respectively.

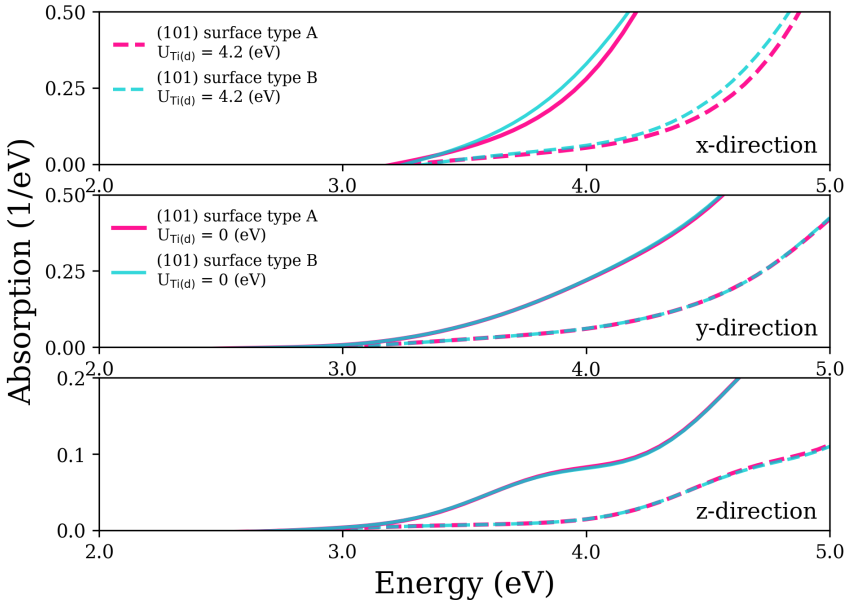

Figure 3. Calculated absorption spectra of a pure TiO_2 (101) surface with and without Hubbard correction $U_{Ti(d)}$. The solid and dashed lines are related to the pure TiO_2 (101) surface with $U_{Ti(d)} = 0$ eV and $U_{Ti(d)} = 4.2$ eV; the pink and cyan colors correspond to the absorption on a doped TiO_2 (101) surface of type A and B. The top, middle, and bottom panels are related to the x, y, and z directions of the orientations of δ-kick.

3.2. Doped Surfaces

Experimental strategies for doping TiO_2 include the hydrothermal method, sol-gel method, co-precipitation method, and electrochemical anodization method. Computational simulation, particularly using DFT and classical molecular dynamics, is also a promising alternative method for studying metal doping in TiO_2 nanotubes [64]. Doping in TiO_2 is primarily done to improve its photocatalytic properties by modifying its electronic structure [65]. Research has focused on doping TiO_2 with transition metals and non-metals to lower the threshold energy for photoexcitation [66]. Various modification strategies for TiO_2 doping include constructing heterojunctions [67]. Metal-doped TiO_2 has shown enhanced photocatalytic activity for dye degradation compared to undoped TiO_2 [68]. In this study, internal positions of Cu in the (101) surfaces of titanium were not considered primarily due to the focus on surface doping effects and their direct impact on the photocatalytic properties of TiO_2. The preference for doping Cu at the surface positions, especially in the (001) surfaces, is based on the significant influence these positions have on enhancing optical absorption and photocatalytic efficiency. Surface doping, particularly in the configuration where Cu substitutes Ti in the surface layer, introduces new mid-gap states that are crucial for lowering the band gap and enhancing light absorption below the band gap of the pure surface. This is particularly important for applications like water splitting and hydrogen production, where efficient light absorption and charge carrier separation are critical. In contrast, internal doping positions might not offer the same level of interaction with incident light or the same degree of influence on the electronic structure at the surface, which is where the photocatalytic reactions predominantly occur. Therefore, this theoretical investigation emphasizes surface doping strategies that directly modify the surface properties of TiO_2 to optimize its photocatalytic performance.

For the copper-doped TiO_2 (101) surface based on the models of types A and B, the DOS is illustrated in Figure 4. When a copper atom is introduced onto the TiO_2 (101) surface using both type A and B models, the resulting changes in the DOS are not significantly different. We observe the formation of mid-gap states caused by the doped Cu atoms that emerged between the original VBM and CBM of the TiO_2 (101) surface. Table 2 lists

positions of levels induced by defects with respect to the top of the valence band as well as the calculated band gap width. Factors contributing to the formation of mid-gap states in Cu-doped TiO_2 surfaces include the localized electronic states of the doped Cu atoms and their interactions with the TiO_2 lattice. The presence of Cu atoms between the original VBM and CBM of the TiO_2 surface leads to the formation of mid-gap states, which are caused by the doped Cu atoms and result in increased absorption below the original band gap of the undoped surface, particularly in the *x* direction. These mid-gap states are crucial for enhancing the absorption in the visible light regions, which is essential for photocatalytic applications. The absorption spectrum of the doped and undoped TiO_2 (101) surfaces for both types A and B is demonstrated in Figure 5. The presence of doped Cu atoms leads to increased absorption below the original band gap of the undoped surface, with the most significant difference observed in the *x* direction. Additionally, we find that the absorption effect is more pronounced in type A surfaces with Cu doping.

Table 2. The band gap width (E_g in eV) and position of defect induced levels in the in-gap state with respect to the top of the valence band (δ in eV) as calculated for (101)- and (001)-terminated Cu-doped nanofilms of anatase TiO_2.

	E_g	δ
TiO_2 (101) surface type A	3.97	0.75
TiO_2 (101) surface type B	4.00	0.77
TiO_2 (001) surface type I	3.32	0.33
TiO_2 (001) surface type II	3.15	0.41
TiO_2 (001) surface type III	3.17	0.27
TiO_2 (001) surface type IV	3.25	0.30

In Figure 6, the DOS for the doped TiO_2 (001) surface is depicted, utilizing four distinct models that differ in the arrangement of the copper atom, which is incorporated in place of titanium. Models I and IV feature copper incorporation in the Ti position within the surface layer of the TiO_2 (001) slab, while models II and III incorporate copper in the subsurface layers.

Models of types I to IV exhibit minimal discrepancies in DOS around the VBM. Table 2 lists positions of defect induced levels with respect to the top of the valence band as well as the calculated band gap width. The pristine TiO_2 (001) surface's VBM edge is characterized by well-defined oxygen states. When examining Cu dopant positions at the top (type I) and bottom (type IV) of the slab, we note the absence of additional states between Cu states and these sharp oxygen states, in contrast with types II and III when Cu is incorporated inside in subsurface layers. The additional tiny oxygen states appear to be split from the original sharp O states of the pure TiO_2 (001) surface.

To understand the impact of this doping, we also examined the absorption spectrum of the doped TiO_2 (001) surface, as illustrated in Figure 7. Similar to the phenomena observed on the (101) surface, the doped Cu atom also induces increased absorption below the original band gap of the pure surface. However, a notable distinction for the TiO_2 (001) surface is that the enhancement in absorption is not confined to the *x* direction; it extends to the *y* and *z* directions as well. The observed slight red shift in the calculated absorption spectra aligns with our recent theoretical investigation involving Cu, Ag, and Au adatoms deposited onto the rutile TiO_2 (110) surface [23]. In cases where the noble metal adatom is not strongly bonded to the surface oxygen or other nearest host surface atoms, the calculated electronic structure of the pristine rutile TiO_2 (110) surface closely resembles that of the surface with an attached adatom. This similarity arises from the contribution of the *d*-orbital of the noble metal adatom, which plays a role in hybridizing the surface states. Specifically, the *sp*-orbitals of the adatom overlap with orbitals at the conduction band of the pristine TiO_2 surface. This hybridization pattern closely mirrors that predicted for Cu-doped anatase TiO_2 surfaces in the current study (see Figures 4 and 6). Consequently,

the process of depositing adatoms on the rutile TiO_2 surface, as well as Cu-doped anatase thin films, can induce localized effects in the optical spectrum.

Considering the absorption properties, three distinct types of transitions can arise from a doped or adsorbed Cu atom. Firstly, the most pronounced enhancement of absorption occurs during the transition from the occupied *sp*-orbitals of Cu to the unoccupied states of the host nanofilm's surface. These transitions result in Cu-induced charge transfer to the TiO_2 surface, closely resembling the optical signatures near the resonance peak of a single Cu atom at approximately 4.8 eV [23]. Secondly, there are transitions from the occupied Cu *d*-orbitals to the unoccupied states of the TiO_2 nanofilm. Given the sufficiently short bond length between Cu and surface oxygen, the optical response of a single Cu atom becomes indistinct or may even be dispelled. Consequently, the occupied Cu *d*-orbitals introduce new transition states at relatively low energies. Thirdly, transitions arise from the occupied states of TiO_2 to the unoccupied Cu *sp*-orbitals. Due to the odd number of Cu electrons, a single occupation occurs at the *sp*-orbitals. This results in the photogenerated electrons of TiO_2 accumulating around the Cu atom. The predicted broader absorption profile underscores the influence of copper doping on the optical properties of TiO_2 surfaces, highlighting the crucial role of surface orientation and doping in modulating the material's absorption characteristics.

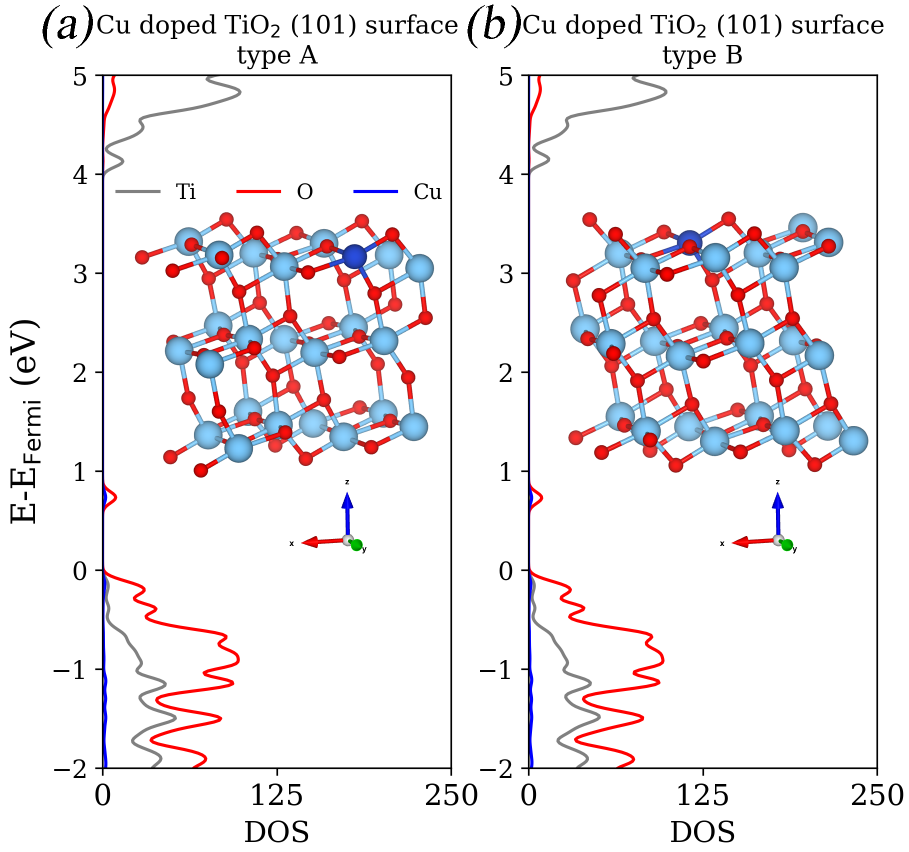

Figure 4. DOS calculated for TiO_2 (101) surface types (**a**) A and (**b**) B. The lines in red, gray, and blue represent the DOS projected onto all orbitals of oxygen (O), titanium (Ti), and copper (Cu) atoms, respectively. The insets of each figure represent the equilibrium atomic structures of the doped surface. The colored balls of red and blue represent the oxygen and titanium atoms, respectively.

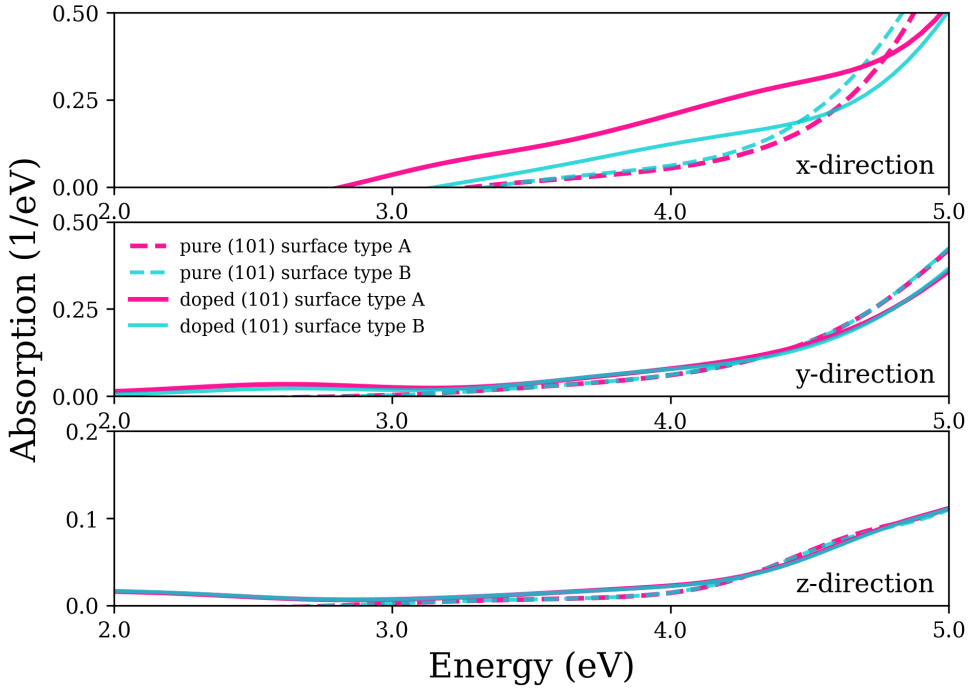

Figure 5. The calculated absorption spectra of pristine and doped TiO_2 (101) surface. The dashed (solid) lines are related to the pristine (doped) TiO_2 (101) surface; the colors pink and cyan correspond to the absorption for a doped TiO_2 (101) surface of types A and B. The top, middle, and bottom panels are related to the x, y, and z directions of the orientations of δ-kick.

In the context of dissociation by photogenerated electrons, this study introduces an alternative strategy that addresses not only enhancements in light absorption but also considerations regarding the final state of electron transitions. It is crucial to comprehend the transition behavior for various deposited elements on the surface, as this understanding plays a pivotal role in harnessing the solar spectrum for future photocatalysts.

It also should be noted that states in the band gap were predicted recently for another promising photocatalytic material used for water splitting and hydrogen production—$SrTiO_3$ nanoparticles doped with Al impurities [69]. These first-principles calculations have shown that Al-induced states serve as hole traps, thus reducing recombination of mobile electrons and holes and respectively increasing the hydrogen production yield. This prediction indeed was confirmed experimentally [70]. In light of these findings, it is reasonable to hypothesize that a similar mechanism might be at play in the case of TiO_2 doped with Cu. This process likely involves carrier trapping, potentially leading to an increase in the efficiency of bacteria destruction. However, this hypothesis warrants further investigation, both theoretically and experimentally.

In summary, the copper doping in TiO_2 surfaces leads to the formation of mid-gap states and thus enhances optical absorption. Incorporating Cu in the surface layer is preferred, as it introduces new mid-gap states that enhance optical absorption below the band gap of the pure surface, which is crucial for photocatalytic applications. It also leads to a broader absorption profile, highlighting the role of surface orientation and doping in modulating the material's light absorption characteristics for applications like water splitting and hydrogen production. It highlights the significance of the preferred doping position for enhancing the photocatalytic efficiency and broadening the application potential of Cu-doped TiO_2 materials. The distinct absorption patterns for different surface orientations and types underscore the complex interplay between doping, surface structure, and optical properties.

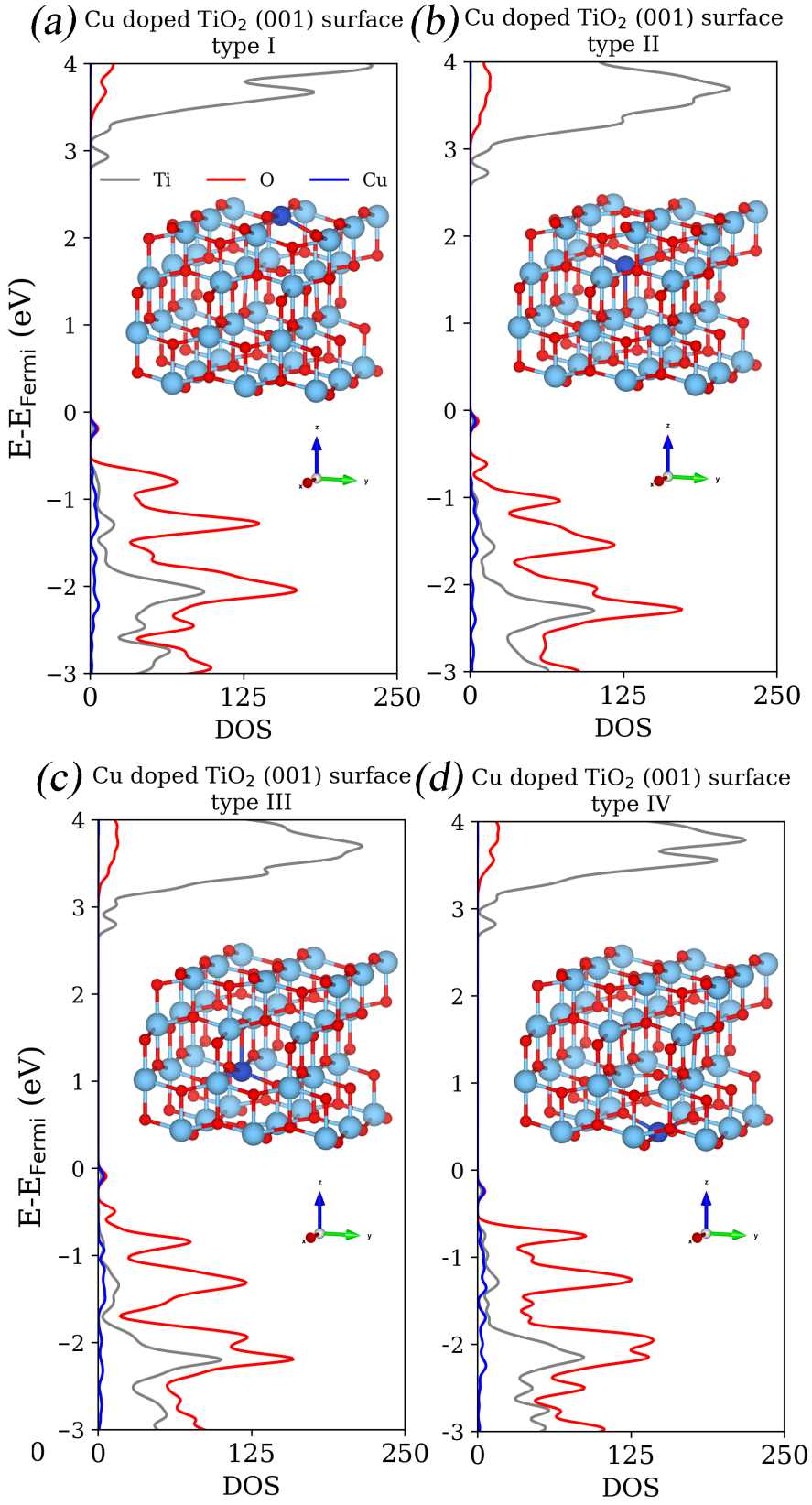

Figure 6. DOS calculated for TiO_2 (001) surface type (**a**) I, (**b**) II, (**c**) III, and (**d**) IV. The lines in red, gray, and blue represent the DOS projected onto all orbitals of oxygen (O), titanium (Ti), and copper (Cu) atoms, respectively. The insets of each figure represent the equilibrium atomic structures of the doped surface. The colored balls in red and blue represent oxygen and titanium atoms, respectively.

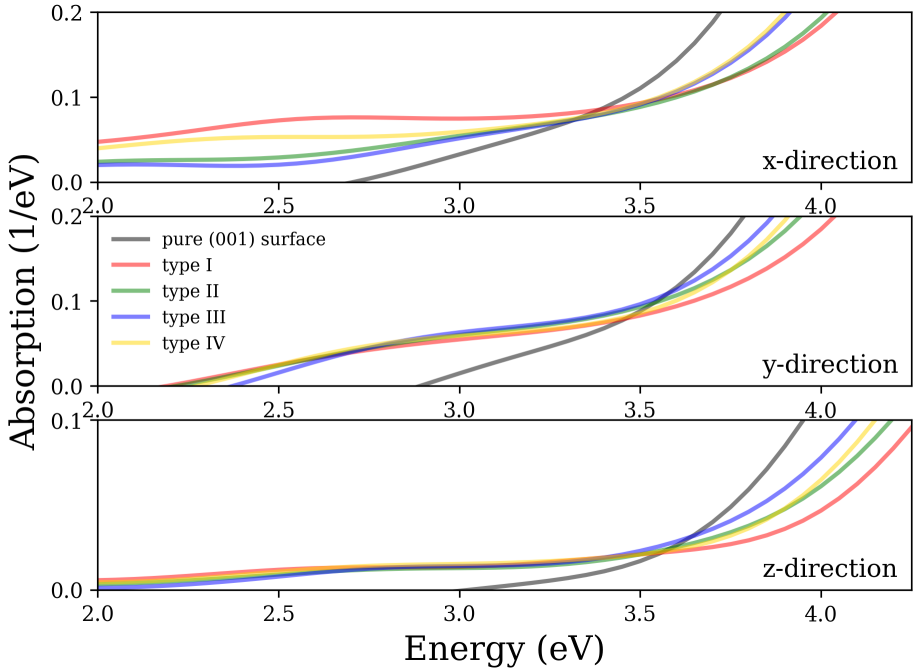

Figure 7. Calculated absorption spectra of pristine and doped TiO_2 (001) surfaces. The black lines are the absorption spectrum of a pristine TiO_2 (001) surface; the colors red, green, blue, and yellow correspond to the absorption predicted for a doped TiO_2 (001) surface of type I, II, III, and IV, respectively. The top, middle, and bottom panels are related to the x, y, and z directions of the orientations of δ-kick.

4. Conclusions

The performed study presents a comprehensive analysis of the electronic structure and optical absorption characteristics of Cu-doped anatase TiO_2 nanofilms, focusing on the (101) and (001) surface terminations. Through state-of-the-art computational methods, we have explored the impact of copper doping on the optical properties of the TiO_2 surface.

The effect of copper-doped surfaces on titanium dioxide can be primarily assessed in terms of energy levels both below and above the band gap of the pure surface. Firstly, a notable enhancement in absorption is observed in both the copper-doped (101) and (001) surfaces for excitation energies below the band gap of the dopant-free surface. This enhancement is attributed to the introduction of new states by the doped Cu atom between the VBM and CBM of the pure surface. Additionally, since the electronic configuration of a single Cu atom occupies states, the TiO_2 surface with a doped Cu atom is conducive to increased absorption in the region below the band gap of the pure surface.

Secondly, doping the TiO_2 surface with copper results in a red shift in the optical absorption spectrum. Analyzing the DOS, it is evident that the doped copper atom brings new hybridizations at the VBM edges, particularly between copper and oxygen states. This hybridization results in smoother oxygen states around the VBM compared to the states of the pure surface, leading to a slightly red-shifted absorption. Additionally, the absorption peak associated with a single Cu atom is located at 4.8 eV [71]. Therefore, the combination of reduced oxygen states around the VBM and the resonance peak of copper contributes to this red shift, especially when the excitation energy surpasses the band gap of the pure surface.

Lastly, TiO_2 nanofilms doped with transition metals like copper hold promise for enhanced photocatalytic and antibacterial properties, consistent with results published previously [72]. These enhancements are crucial, offering significant implications for public health by mitigating the spread of harmful microorganisms and presenting opportunities for the development of novel photocatalytic materials, particularly for applications such as water splitting and hydrogen production.

Author Contributions: Conceptualization, Y.-P.L., E.N., H.B. and D.B.; methodology, Y.-P.L., E.N., D.B. and S.P.; software, Y.-P.L.; validation, Y.-P.L., E.N., D.B., H.B., E.A.K. and S.P.; formal analysis, Y.-P.L., E.N., D.B., E.A.K., H.B., S.Z. and S.P.; investigation, Y.-P.L. and E.N.; resources, E.A.K., D.B. and S.P.; data curation, Y.-P.L., E.N., D.B. and S.P.; writing—original draft preparation, Y.-P.L. and E.N.; writing—review and editing, E.A.K., H.B., S.Z., I.I., S.P. and D.B.; visualization, Y.-P.L.; supervision, E.A.K., D.B. and S.P.; project administration, I.I., H.B. and D.B.; funding acquisition, E.A.K., D.B., H.B. and S.P. All authors have read and agreed to the published version of the manuscript.

Funding: This study was financially supported by Flag-ERA JTC To2Dox project. E.N. and D.B. thank the Latvian Scientific Council grant No. LZP-2021/1-0464 for support. H.B. and S.Z. are thankful for support from the State Program for Scientific Research of Belarus «Photonics and electronics for innovations». Y.-P.L. thanks the M-ERA.NET project "Multiscale computer modelling, synthesis and rational design of photo(electro)catalysts for efficient visible-light-driven seawater splitting" (CatWatSplit) for financial support. The Institute of Solid State Physics, University of Latvia, as the Center of Excellence, has received funding from the European Union's Horizon 2020 Framework Program H2020-WIDESPREAD-01-2016-2017-TeamingPhase2 under Grant Agreement No. 739508, project CAMART^2. The calculations were performed at the Latvian SuperCluster (LASC), located at the Institute of Solid State Physics, University of Latvia.

Data Availability Statement: The raw/processed data required to reproduce these findings cannot be shared at this time, as the data also form part of an ongoing study.

Conflicts of Interest: The authors declare no conflicts of interest. The funders had no role in the design of the study; in the collection, analyses, or interpretation of data; in the writing of the manuscript; or in the decision to publish the results.

References

1. Al-Hazmi, F.; Alnowaiser, F.; Al-Ghamdi, A.; Al-Ghamdi, A.A.; Aly, M.; Al-Tuwirqi, R.M.; El-Tantawy, F. A new large—Scale synthesis of magnesium oxide nanowires: Structural and antibacterial properties. *Superlattices Microstruct.* **2012**, *52*, 200–209. [CrossRef]
2. Lopez de Dicastillo, C.; Correa, M.; Martínez, F.; Streitt, C.; Galotto, M. Antimicrobial Effect of Titanium Dioxide Nanoparticles. In *Antimicrobial Resistance—A One Health Perspective* ; IntechOpen: London, UK, 2020. [CrossRef]
3. Maeda, K. Photocatalytic water splitting using semiconductor particles: History and recent developments. *J. Photochem. Photobiol. C* **2011**, *12*, 237–268. [CrossRef]
4. Li, B.; Wu, S.; Gao, X. Theoretical calculation of a TiO_2-based photocatalyst in the field of water splitting: A review. *Nanotechnol. Rev.* **2020**, *9*, 1080–1103. [CrossRef]
5. Serga, V.; Burve, R.; Krumina, A.; Romanova, M.; Kotomin, E.A.; Popov, A.I. Extraction–pyrolytic method for TiO_2 polymorphs production. *Crystals* **2021**, *11*, 431. [CrossRef]
6. Zhang, W.; Liu, H.; Liu, Z.; An, Y.; Zhong, Y.; Hu, Z.; Li, S.; Chen, Z.; Wang, S.; Sheng, X.; et al. Eu-doped zeolitic imidazolate framework-8 modified mixed-crystal TiO_2 for efficient removal of basic fuchsin from effluent. *Materials* **2021**, *14*, 7265. [CrossRef] [PubMed]
7. Ho, V.T.T.; Chau, D.H.; Bui, K.Q.; Nguyen, N.T.T.; Tran, T.K.N.; Bach, L.G.; Truong, S.N. A high-performing nanostructured Ir doped-TiO_2 for efficient photocatalytic degradation of gaseous toluene. *Inorganics* **2022**, *10*, 29. [CrossRef]
8. Permporn, D.; Khunphonoi, R.; Wilamat, J.; Khemthong, P.; Chirawatkul, P.; Butburee, T.; Sangkhun, W.; Wantala, K.; Grisdanurak, N.; Santatiwongchai, J.; et al. Insight into the roles of metal loading on CO_2 photocatalytic reduction behaviors of TiO_2. *Nanomaterials* **2022**, *12*, 474. [CrossRef] [PubMed]
9. Tsebriienko, T.; Popov, A.I. Effect of poly(titanium oxide) on the viscoelastic and thermophysical properties of interpenetrating polymer networks. *Crystals* **2021**, *11*, 794. [CrossRef]
10. Fujishima, A.; Zhang, X.; Tryk, D.A. TiO_2 photocatalysis and related surface phenomena. *Surf. Sci. Rep.* **2008**, *63*, 515–582. [CrossRef]
11. Danish, M.S.S.; Estrella, L.L.; Alemaida, I.M.A.; Lisin, A.; Moiseev, N.; Ahmadi, M.; Nazari, M.; Wali, M.; Zaheb, H.; Senjyu, T. Photocatalytic applications of metal oxides for sustainable environmental eemediation. *Metals* **2021**, *11*, 80. [CrossRef]
12. Huang, H.; Huang, H.; Zhang, L.; Hu, P.; Ye, X.; Leung, D.Y. Enhanced degradation of gaseous benzene under vacuum ultraviolet (VUV) irradiation over TiO_2 modified by transition metals. *Chem. Eng. J.* **2015**, *259*, 534–541. [CrossRef]
13. Dong, H.; Zeng, G.; Tang, L.; Fan, C.; Zhang, C.; He, X.; He, Y. An overview on limitations of TiO_2-based particles for photocatalytic degradation of organic pollutants and the corresponding countermeasures. *Water Res.* **2015**, *79*, 128–146. [CrossRef]
14. Serga, V.; Burve, R.; Krumina, A.; Pankratova, V.; Popov, A.I.; Pankratov, V. Study of phase composition, photocatalytic activity, and photoluminescence of TiO_2 with Eu additive produced by the extraction-pyrolytic method. *J. Mater. Res. Technol.* **2021**, *13*, 2350–2360. [CrossRef]

15. Zhukovskii, Y.F.; Piskunov, S.; Lisovski, O.; Bocharov, D.; Evarestov, R.A. Doped 1D nanostructures of transition-metal oxides: First-principles evaluation of photocatalytic suitability. *Isr. J. Chem.* **2017**, *57*, 461–476. [CrossRef]
16. Alfaifi, B.Y.; Ullah, H.; Alfaifi, S.Y.; Tahir, A.A.; Mallick, T.K. Photoelectrochemical solar water splitting: From basic principles to advanced devices. *Veruscript Funct. Nanomater.* **2018**, *2*, BDJOC3. [CrossRef]
17. Pham, T.D.; Lee B.-K. Effects of Ag doping on the photocatalytic disinfection of *E. coli* in bioaerosol by Ag–TiO_2/GF under visible light. *J. Colloid Interface Sci.* **2014**, *428*, 24–31. [CrossRef] [PubMed]
18. Pham, T.D.; Lee B.-K. Cu doped TiO_2/GF for photocatalytic disinfection of *Escherichia coli* in bioaerosols under visible light irradiation: Application and mechanism. *Appl. Surf. Sci.* **2014**, *296*, 9. [CrossRef]
19. Foster, H.; Ditta, I.; Varghese, S.; Steele, A. Photocatalytic disinfection using titanium dioxide: Spectrum and mechanism of antimicrobial activity. *Appl. Microbiol. Biotechnol.* **2011**, *90*, 1847–1868. [CrossRef] [PubMed]
20. Tanabe, I.; Ozaki, Y. Far- and deep-ultraviolet spectroscopic investigations for titanium dioxide: Electronic absorption, Rayleigh scattering, and Raman spectroscopy. *J. Mater. Chem. C* **2016**, *4*, 7706–7717. [CrossRef]
21. Mathew, S.; Ganguly, P.; Rhatigan, S.; Kumaravel, V.; Byrne, C.; Hinder, S.; Bartlett, J.; Nolan, M.; Pillai, S. Cu-Doped TiO_2: Visible Light Assisted Photocatalytic Antimicrobial Activity. *Appl. Sci.* **2018**, *8*, 2067. [CrossRef]
22. Wang, C.; Hu, Q.; Huang, J.; Zhu, C.; Deng, Z.; Shi, H.; Wu, L.; Liu, Z.; Cao, Y. Enhanced hydrogen production by water splitting using Cu-doped TiO_2 film with preferred (0 0 1) orientation. *Appl. Surf. Sci.* **2014**, *292*, 161–164. [CrossRef]
23. Lin, Y.P.; Bocharov, D.; Kotomin, E.A.; Brik, M.G.; Piskunov, S. Influence of Au, Ag, and Cu Adatoms on Optical Properties of TiO_2 (110) Surface: Predictions from RT-TDDFT Calculations. *Crystals* **2022**, *12*, 452. [CrossRef]
24. Kamalov, R.; Vokhmintsev, A.; Dorosheva, I.; Kravets, N.; Weinstein, I. Synthesis of Composite Based on Carbon Nanotubes and Anodic Titania. *Adv. Sci. Lett.* **2016**, *22*, 688–690. [CrossRef]
25. Kukli, K.; Lu, J.; Link, J.; Kemell, M.; Puukilainen, E.; Heikkilä, M.; Hoxha, R.; Tamm, A.; Hultman, L.; Stern, R.; et al. Holmium and titanium oxide nanolaminates by atomic layer deposition. *Thin Solid Films* **2014**, *565*, 165–171. [CrossRef]
26. Wang, Y.; Wang, X.; Li, L.; Wu, Y.; Yu, Q. An experimental and theoretical study on the photocatalytic antibacterial activity of boron-doped TiO_2 nanoparticles. *Ceram. Int.* **2021**, *48*, 604–614. [CrossRef]
27. Alisiyonak, O.; Lavitskaya, A.; Khoroshko, L.; Kozlovskiy, A.L.; Zdorovets, M.; Korolkov, I.; Yauseichuk, M.; Kaniukov, E.; Shumskaya, A. Breathable Films with Self-Cleaning and Antibacterial Surfaces Based on TiO_2-Functionalized PET Membranes. *Membranes* **2023**, *13*, 733. [CrossRef]
28. Dukenbayev, K.; Kozlovskiy, A.; Kenzhina, I.; Berguzinov, A.; Zdorovets, M. Study of the effect of irradiation with Fe^{7+} ions on the structural properties of thin TiO_2 foils. *Mater. Res. Express* **2019**, *6*, 046309. [CrossRef]
29. Kozlovskiy, A.; Shlimas, I.; Dukenbayev, K.; Zdorovets, M. Structure and corrosion properties of thin TiO_2 films obtained by magnetron sputtering. *Vacuum* **2019**, *164*, 224–232. [CrossRef]
30. Zdorovets, M.; Kozlovskiy, A.; Tishkevich, D.; Zubar, T.; Trukhanov, A. The effect of doping of TiO_2 thin films with low-energy O^{2+} ions on increasing the efficiency of hydrogen evolution in photocatalytic reactions of water splitting. *J. Mater. Sci. Mater. Electron.* **2020**, *31*, 21142–21153. [CrossRef]
31. Wang, Z.; Labat, F. Modeling stoichiometric and oxygen defective TiO_2 anatase bulk and (101) surface: Structural and electronic properties from hybrid DFT. *J. Mol. Model.* **2023**, *29*, 174. [CrossRef] [PubMed]
32. Harb, M.; Sautet, P.; Raybaud, P. Anionic or Cationic S-Doping in Bulk Anatase TiO_2: Insights on Optical Absorption from First Principles Calculations. *J. Phys. Chem. C* **2013**, *117*, 8892–8902. [CrossRef]
33. Gustavsen, K.; Feng, T.; Huang, H.; Li, G.; Narkiewicz, U.; Wang, K. DFT Calculation of Carbon-Doped TiO_2 Nanocomposites. *Materials* **2023**, *16*, 6117. [CrossRef]
34. Fu, C.; Liu, L.; Li, Z.; Wei, Y.; Huang, W.; Zhang, X. Synergy of Bulk Defects and Surface Defects on TiO_2 for Highly Efficient Photocatalytic Production of H_2O_2. *J. Phys. Chem. Lett.* **2023**, *14*, 7690–7696. [CrossRef] [PubMed]
35. Zavatski, S.; Neilande, E.; Bandarenka, H.; Popov, A.I.; Piskunov, S.; Bocharov, D. Density functional theory for doped TiO_2: Current research strategies and advancements. *Nanotechnology* **2024**, *35*, 192001. [CrossRef]
36. Pilar de Lara-Castells, M.; Hauser, A.W.; Ramallo-López, J.M.; Buceta, D.; Giovanetti, L.J.; López-Quintela, M.A.; Requejo, F.G. Increasing the optical response of TiO_2 and extending it into the visible region through surface activation with highly stable Cu_5 clusters. *J. Mater. Chem. A* **2019**, *7*, 7489–7500. [CrossRef]
37. López-Caballero, P.; Ramallo-López, J.M.; Giovanetti, L.J.; Buceta, D.; Miret-Artés, S.; López-Quintela, M.A.; Requejo, F.G.; de Lara-Castells, M.P. Exploring the properties of Ag_5–TiO_2 interfaces: Stable surface polaron formation, UV-Vis optical response, and CO_2 photoactivation. *J. Mater. Chem. A* **2020**, *8*, 6842–6853. [CrossRef]
38. Yuan, W.; Zhu, B.; Li, X.Y.; Hansen, T.W.; Ou, Y.; Fang, K.; Yang, H.; Zhang, Z.; Wagner, J.B.; Gao, Y.; et al. Visualizing H_2O molecules reacting at TiO_2 active sites with transmission electron microscopy. *Science* **2020**, *367*, 428–430. [CrossRef]
39. de Lara-Castells, M.P.; Cabrillo, C.; Micha, D.A.; Mitrushchenkov, A.O.; Vazhappilly, T. Ab initio design of light absorption through silver atomic cluster decoration of TiO_2. *Phys. Chem. Chem. Phys.* **2018**, *20*, 19110–19119. [CrossRef]
40. Kenmoe, S.; Lisovski, O.; Piskunov, S.; Zhukovskii, Y.F.; Spohr, E. Electronic and optical properties of pristine, N- and S-doped water-covered TiO_2 nanotube surfaces. *J. Chem. Phys.* **2019**, *150*, 041714. [CrossRef] [PubMed]
41. Rossi, T.P.; Kuisma, M.; Puska, M.J.; Nieminen, R.M.; Erhart, P. Kohn–Sham decomposition in real-time time-dependent density-functional theory: An efficient tool for analyzing plasmonic excitations. *J. Chem. Theory Comput.* **2017**, *13*, 4779–4790. [CrossRef]

42. Conley, K.M.; Nayyar, N.; Rossi, T.P.; Kuisma, M.; Turkowski, V.; Puska, M.J.; Rahman, T.S. Plasmon excitations in mixed metallic nanoarrays. *ACS Nano* **2019**, *13*, 5344–5355. [CrossRef] [PubMed]
43. Rossi, T.P.; Shegai, T.; Erhart, P.; Antosiewicz, T.J. Strong plasmon-molecule coupling at the nanoscale revealed by first-principles modeling. *Nat. Commun.* **2019**, *10*, 3336. [CrossRef] [PubMed]
44. Mokkath, J.H. Strong collectivity of optical transitions in lead halide perovskite quantum dots. *Plasmonics* **2020**, *15*, 581–590. [CrossRef]
45. Qu, Z.W.; Kroes, G.J. Theoretical study of adsorption of O(3P) and H_2O on the rutile TiO_2(110) surface. *J. Phys. Chem. B* **2006**, *110*, 23306–23314. [CrossRef] [PubMed]
46. Enkovaara, J.; Rostgaard, C.; Mortensen, J.; Chen, J.; Dulak, M.; Ferrighi, L.; Gavnholt, J.; Glinsvad, C.; Haikola, V.; Hansen, H.; et al. Electronic structure calculations with GPAW: A real-space implementation of the projector augmented-wave method. *J. Condens. Matter Phys.* **2010**, *22*, 253202. [CrossRef] [PubMed]
47. Walter, M.; Häkkinen, H.; Lehtovaara, L.; Puska, M.; Enkovaara, J.; Rostgaard, C.; Mortensen, J. Time-dependent density-functional theory in the projector augmented-wave method. *J. Chem. Phys.* **2008**, *128*, 244101. [CrossRef]
48. Larsen, A.; Mortensen, J.; Blomqvist, J.; Castelli, I.; Christensen, R.; Dulak, M.; Friis, J.; Groves, M.; Hammer, B.; Hargus, C.; et al. The Atomic Simulation Environment — A Python library for working with atoms. *J. Condens. Matter Phys.* **2017**, *29*, 273002. [CrossRef] [PubMed]
49. Kuisma, M.; Sakko, A.; Rossi, T.; Larsen, A.; Enkovaara, J.; Lehtovaara, L.; Rantala, T. Localized surface plasmon resonance in silver nanoparticles: Atomistic first-principles time-dependent density-functional theory calculations. *Phys. Rev. B* **2015**, *91*, 115431. [CrossRef]
50. Makkonen, E.; Rossi, T.; Larsen, A.; Acevedo, O.L.; Rinke, P.; Kuisma, M.; Chen, x. Real-time time-dependent density functional theory implementation of electronic circular dichroism applied to nanoscale metal–organic clusters. *J. Chem. Phys.* **2021**, *154*, 114102. [CrossRef]
51. Ivanov, A.V.; Jónsson, E.Ö.; Vegge, T.; Jónsson, H. Direct energy minimization based on exponential transformation in density functional calculations of finite and extended systems. *Comput. Phys. Commun.* **2021**, *267*, 108047. [CrossRef]
52. Perdew, J.; Burke, K.; Ernzerhof, M. Generalized Gradient Approximation Made Simple. *Phys. Rev. Lett.* **1996**, *77*, 3865–3868. [CrossRef] [PubMed]
53. Larsen, A.H.; Vanin, M.; Mortensen, J.J.; Thygesen, K.S.; Jacobsen, K.W. Localized atomic basis set in the projector augmented wave method. *Phys. Rev. B* **2009**, *80*, 195112. [CrossRef]
54. Kuisma, M.; Ojanen, J.; Enkovaara, J.; Rantala, T.T. Kohn-Sham potential with discontinuity for band gap materials. *Phys. Rev. B* **2010**, *82*, 115106. [CrossRef]
55. Castelli, I.E.; Hüser, F.; Pandey, M.; Li, H.; Thygesen, K.S.; Seger, B.; Jain, A.; Persson, K.A.; Ceder, G.; Jacobsen, K.W. New Light-Harvesting Materials Using Accurate and Efficient Bandgap Calculations. *Adv. Energy Mater.* **2015**, *5*, 1400915. [CrossRef]
56. Momma, K.; Izumi, F. VESTA 3 for Three-Dimensional Visualization of Crystal, Volumetric and Morphology Data. *J. Appl. Crystallogr.* **2011**, *44*, 1272–1276. [CrossRef]
57. van der Walt, S.; Colbert, S.; Varoquaux, G. The NumPy Array: A Structure for Efficient Numerical Computation. *Comput. Sci. Eng.* **2011**, *13*, 22–30. [CrossRef]
58. Hunter, J. Matplotlib: A 2D Graphics Environment. *Comput. Sci. Eng.* **2007**, *9*, 90–95. [CrossRef]
59. Himmetoglu, B.; Floris, A.; De Gironcoli, S.; Cococcioni, M. Hubbard-corrected DFT energy functionals: The LDA+U description of correlated systems. *Int. J. Quantum Chem.* **2014**, *114*, 14–49. [CrossRef]
60. Tritsaris, G.; Vinichenko, D.; Kolesov, G.; Friend, C.; Kaxiras, E. Dynamics of the Photogenerated Hole at the Rutile TiO_2(110)/Water Interface: A Nonadiabatic Simulation Study. *J. Phys. Chem. C* **2014**, *118*, 27393–27401. [CrossRef]
61. Deng, Q.; Zhang, W.; Lan, T.; Xie, J.; Xie, W.; Liu, Z.; Huang, Y.; Wei, M. Anatase TiO_2 quantum dots with a narrow bandgap energy of 2.85 eV exhibiting significant photodegradation property. *Eur. J. Inorg. Chem.* **2018**, *2018*, 1506–1510. [CrossRef]
62. Lin, Y.P.; Bocharov, D.; Isakoviča, I.; Pankratov, V.; Popov, A.A.; Popov, A.I.; Piskunov, S. Chlorine Adsorption on TiO_2 (110)/Water Interface: Nonadiabatic Molecular Dynamics Simulations for Photocatalytic Water Splitting. *Electron. Mater.* **2023**, *4*, 33–48. [CrossRef]
63. Lin, Y.P.; Isakoviča, I.; Gopejenko, A.; Ivanova, A.; Začinskis, A.; Eglitis, R.I.; D'yachkov, P.N.; Piskunov, S. Time-dependent density functional theory calculations of N- and S-doped TiO_2 nanotube for water-splitting applications. *Nanomaterials* **2021**, *11*, 2900. [CrossRef] [PubMed]
64. Estévez Ruiz, E.P.; Lago, J.L.; Thirumuruganandham, S.P. Experimental Studies on TiO_2 NT with Metal Dopants through Co-Precipitation, Sol–Gel, Hydrothermal Scheme and Corresponding Computational Molecular Evaluations. *Materials* **2023**, *16*, 3076. [CrossRef] [PubMed]
65. Carey, J.J.; McKenna, K.P. Screening doping strategies to mitigate electron trapping at anatase TiO_2 surfaces. *J. Phys. Chem. C* **2019**, *123*, 22358–22367. [CrossRef] [PubMed]
66. Di Valentin, C.; Finazzi, E.; Pacchioni, G.; Selloni, A.; Livraghi, S.; Paganini, M.C.; Giamello, E. N-doped TiO_2: Theory and experiment. *Chem. Phys.* **2007**, *339*, 44–56. [CrossRef]
67. Humayun, M.; Raziq, F.; Khan, A.; Luo, W. Modification strategies of TiO_2 for potential applications in photocatalysis: A critical review. *Green Chem. Lett. Rev.* **2018**, *11*, 86–102. [CrossRef]

68. Sultana, M.; Mondol, A.; Islam, S.; Khatun, M.A.; Rahman, M.H.; Chakraborty, A.K.; Rahman, M.S.; Rahman, M.M.; Nur, A.S. Strategic development of metal doped TiO_2 photocatalysts for enhanced dye degradation activity under UV–Vis irradiation: A review. *Curr. Res. Green Sustain. Chem.* **2023**, *7*, 100383. [CrossRef]
69. Rusevich, L.L.; Kotomin, E.A.; Zvejnieks, G.; Kržmanc, M.M.; Gupta, S.; Daneu, N.; Wu, J.C.; Lee, Y.G.; Yu, W.Y. Effects of Al Doping on Hydrogen Production Efficiency upon Photostimulated Water Splitting on $SrTiO_3$ Nanoparticles. *J. Phys. Chem. C* **2022**, *126*, 21223–21233. [CrossRef]
70. Tai, Y.Y.; Wu, J.C.; Yu, W.Y.; Kržmanc, M.M.; Kotomin, E. Photocatalytic water splitting of improved strontium titanate for simultaneous separation of H_2 in a twin photoreactor. *Appl. Catal. B* **2023**, *324*, 122183. [CrossRef]
71. LeCoultre, S.; Rydlo, A.; Félix, C.; Buttet, J.; Gilb, S.; Harbich, W. Optical absorption of small copper clusters in neon: Cu_n, (n = 1–9). *J. Chem. Phys.* **2011**, *134*, 074303. [CrossRef]
72. Zhang, E.; Wang, X.; Chen, M.; Hou, B. Effect of the existing form of Cu element on the mechanical properties, bio-corrosion and antibacterial properties of Ti-Cu alloys for biomedical application. *Mater. Sci. Eng. C* **2016**, *69*, 1210–1221. [CrossRef] [PubMed]